# Visual Auto-landing of an Autonomous Aircraft

Patrick Rives, José Raul Azinheira

INRIA

INSTITUT NATIONAL DE RECHERCHE EN INFORMATIQUE ET EN AUTOMATIQUE

# *Visual Auto-landing of an Autonomous Aircraft*

Patrick Rives — José Raul Azinheira

**N° 4606**

Novembre 2002

THÈME 4


ISSN 0249-6399 ISRN INRIA/RR--4606--FR+ENG

INRIA
SOPHIA ANTIPOLIS

# Visual Auto-landing of an Autonomous Aircraft

Patrick Rives *, José Raul Azinheira †

Thème 4 — Simulation et optimisation
de systèmes complexes
Projet Icare

Rapport de recherche n° 4606 — Novembre 2002 — 44 pages

**Abstract:** This report is the summary of work done in the CIMAR project of collaboration between IST (Lisboa) and the Icare Project (INRIA Sophia Antipolis) for vision-based control applied to an autonomous aircraft.
An unified modeling framework is defined and the vision-based auto-landing of the UAV model is analyzed, based on the classical alternative between position-based and image-based visual control. The controller design is adapted for both approaches and simulations results are presented in order to validate the proposed solutions and allow for a critical evaluation of the two approaches.

**Key-words:** Unmanned Aerial Vehicle UAV, Vision-based control, auto-landing, dynamic modeling, robust control

* INRIA Sophia Antipolis
† Instituto Superior Técnico - IDMEC/IST (Lisbonne)

Unité de recherche INRIA Sophia Antipolis
2004, route des Lucioles, BP 93, 06902 Sophia Antipolis Cedex (France)
Téléphone : +33 4 92 38 77 77 — Télécopie : +33 4 92 38 77 65

# Atterrissage automatique par asservissement visuel

**Résumé :** Ce rapport est la synthèse du travail réalisé dans le cadre du projet de collaboration *Cimar* entre le projet *Icare* de l'INRIA et le Groupe de Contrôle de l' *Instituto Superior Técnico* de Lisbonne. Ce travail compare deux approches d'asservissement visuel (position-based et image-based) appliquées au contrôle d'un drône aérien dans une phase d'atterrissage automatique. La difficulté du problème réside principalement dans le modèle dynamique fortement non linéaire et couplé du drône ARMOR X7 UAV qui peut amener à des instabilités lorsqu'on le reboucle avec des informations visuelles. Les aspects modélisations et synthèse des controleurs pour les deux approches sont présentés et comparés en simulation

**Mots-clés :** Asservissement visuel, modéle dynamique de drône aérien, atterrissage automatique, controleur LQR

# 1 Introduction

The main objective of the present work is the search for control strategies for the automatic landing of an autonomous air vehicle using the images provided by an airborne camera.

The landing is the more demanding flight phase, both in terms of required accuracy and necessary robustness. Another characteristic of the landing (partly justifying the previous statement) is the fact that the relevant position variables are relative to a local ground frame, inside of which the vehicle has to be taken safely from the flying condition to the touchdown and then rolling on the ground.

The problem may be considered as the extreme case of a need of perfect path tracking in a ground relative frame, for which a vision sensor (an airborne camera) may be regarded as a sensor with adequate characteristics, that may be useful for the precise positioning relatively to the ground.

In terms of control strategy two extreme options are available:

- a first solution, referred as the position-based visual servoing or reconstruction approach, consists in considering the image output as just another sensor specifically used to help for the landing phase in order to get a better estimate of the vehicle position, as compared to a pretended landing path;
- a second solution, so called image-based visual servoing approach, consists in switching from the flight control scheme to a landing scheme where the vehicle motion is only referenced to the image as compared to a reference image to be tracked.

The position-based visual servoing approach is a more conservative solution, probably easier to implement: the flight control scheme is almost unchanged and extended to the landing phase, only switching to an image enhanced estimation of the position. On the other hand the reconstruction relies on a good calibration of the camera and the effect of the image noise or inaccuracy must be secured.

Some papers already touched the problem of vision based flight control, like [chat98] or [kimm02]. The first paper presents a pose reconstruction technique to be used as a pilot aid during landing, with no automatic control. The second one is more recent and presents the simulation results of a reconstruction control scheme for in-flight refueling.

The image-based visual servoing approach is more ambitious and a cautious analysis is required before it may be tested in real flight conditions. It must be verified that the control in the image does not excite the unstable or marginally stable dynamics of the vehicle. It is however a solution that is not so dependent on the camera calibration, as long as an acceptable reference image is produced for the visual tracking [esp92], [riv96]. In contrast with the usual image-based control in robotics, in our particular case the target system may not be assumed as a pure velocity integrator, the aircraft is under-actuated and its dynamics and the couplings between the axes may not be neglected and are to be integrated into the controller design.

The report is structured as follows. In a first section, we briefly present the dynamic model of the aircraft, which will be used for the controllers design. The second section is devoted to the image modeling and introduces the two different visual servoing approaches which will be detailed in the third and fourth sections respectively. Finally the fifth section presents simulation results which allow to discuss the advantages and drawbacks of each approach.

# 2 Dynamic Modeling of the Aircraft

A more detailed description of the ARMOR X7 model may be found in the technical report of Nuno Costa [cos99]. Most of the notions presented hereafter may be found in the bibliography on Flight Mechanics, namely in the following references: Stevens [ste92], MacLean [mcl90] or McCormick [mcc95].

## 2.1 Frames and Notations

The trajectory of the aircraft and the coordinates of the landing field elements are given in the earth frame (or NED, for North-East-Down), with the center by instance on the field axis. The local frame, linked to the aircraft body (ABC, aircraft body centered), where the aircraft velocity $V = [u, v, w]^T$ is given, is centered at its center of gravity (O), $u$ directed towards the aircraft nose, $v$ towards the right wing and $w$ to down. The angular velocity is also expressed in the local frame: $\Omega = [p, q, r]^T$. The change from the earth frame to the local frame is defined by the transformation matrix $S$, which may be stated in terms of the Euler angles $[\phi, \theta, \psi]^T$, respectively roll, pitch and yaw angles, that may individually be viewed as the rotations around each one of the local frame axes. As an alternative, matrix S may be expressed in terms of the quaternions $[e_0, e_1, e_2, e_3]^T$, which has the advantage of resulting in a continuous representation with algebraic relations.

## 2.2 Flight Mechanics and Dynamic Modeling

The atmospheric flight is generally deduced from the application of Newton's second law, considering the motion of the aircraft in the earth frame, assumed as an inertial frame, under the influence of forces and torques due to gravity $(F_g, 0)$, aerodynamics $(F_a, M_a)$ and propulsion $(F_p, M_p)$ :

$$\frac{d(mV)}{dt}_{NED} = F_g + F_a + F_p \tag{1}$$

$$\frac{d(I\Omega)}{dt}_{NED} = M_a + M_p \tag{2}$$

where $V$ is the velocity of the aircraft center of gravity (O) and $\Omega$ is the angular velocity, $m$ is the aircraft mass and $I$ its inertial matrix.

The change from earth frame to local frame introduces the Coriolis acceleration:

$$\frac{d}{dt}_{NED} = \frac{d}{dt}_{ABC} + \Omega \times \tag{3}$$

If the mass and inertial matrix are assumed as constant (or vary very slowly) and if all the variables are represented in the local frame, one finally obtains the two following differential equations:

$$\frac{dV}{dt} = -\Omega \times V + \frac{1}{m}(F_g + F_a + F_p) \tag{4}$$

$$\frac{d\Omega}{dt} = -I^{-1}\Omega \times I\Omega + I^{-1}(M_a + M_p) \tag{5}$$

In order to proceed with the analysis, it is necessary to establish the link between applied forces or torques and the problem variables.

### 2.2.1 Gravity

The gravity acceleration is expressed in the earth frame $G = [0, 0, g]^T$. The gravity force (weight) $F_g$ only depends on the transformation matrix $S$ : $F_g = mSG$, and therefore on the angular position of the aircraft. The cinematic relation between this angular position and its derivatives gives another differential equation:

$$\frac{dS}{dt} = -\Omega \times S \tag{6}$$

which may be expressed in terms of Euler angles or quaternions.

### 2.2.2 Aerodynamics and Propulsion

The forces and torques due to aerodynamics and propulsion depend mostly on the air velocity $V_a$, relative velocity of the aircraft in the air, obtained from the difference between absolute velocity $V$ and wind velocity $V_w$ :

$$V_a = V - V_w \tag{7}$$

The air velocity is often expressed in spherical coordinates, introducing the airspeed $V_T = \|V_a\|$ (True Air Speed -TAS), and the two aerodynamic angles, the angle of attack $\alpha$ in the vertical plane and the side slip angle $\beta$ in the horizontal plane.

The influence of the air velocity on the aircraft motion is non linear and also depends on the time derivatives and angular rates.

The forces due to aerodynamics finally depend on the input variables that allow to control the system (the aircraft). For the aerodynamic forces, in the case of a conventional aircraft, the inputs are: the angular deflection of the ailerons $\delta_a$, the deflection of the elevators $\delta_e$ and the rudder deflection $\delta_r$.

Giving thus:

$$\overline{F}_a = \overline{F}_a(V_T, \alpha, \beta, p, q, r, \delta_a, \delta_e, \delta_r) \tag{8}$$

where $\overline{F}$ is the vector representing the force and torque due to aerodynamics.

For the propulsion, as a first approach, the thrust produced by the propeller, assumed as aligned with the aircraft longitudinal axis, is taken as the control input, giving thus :

$$\overline{F}_p = \overline{F}_p(V_T, \alpha, \beta, p, q, r, T) \tag{9}$$

The form and values of both generalized forces $\overline{F}_a$ and $\overline{F}_p$ are obtained experimentally or from empirical laws.

### 2.2.3 State Equations

If the expressions of forces and applied torques are introduced, three differential vectorial equations result, representing the equations of the system dynamics :

$$\begin{cases} \frac{dV}{dt} = -\Omega \times V + SG + \frac{1}{m}(F_a + F_p) \\ \frac{d\Omega}{dt} = -I^{-1}\Omega \times I\Omega + I^{-1}(M_a + M_p) \\ \frac{dS}{dt} = -\Omega \times S \end{cases} \tag{10}$$

which may be put in a synthetic form as the following state space dynamic equation:

$$\dot{X} = f(X, U, D) \tag{11}$$

where:

- $\dot{X} = \frac{dX}{dt}$ is the concise notation for the time derivative
- the state may be expressed in terms of the Euler angles $X^T = [u, v, w, p, q, r, \phi, \theta, \psi]$ or with the quaternions $X^T = [u, v, w, p, q, r, e_0, e_1, e_2, e_3]$
- the input vector is $U^T = [\delta_a, \delta_e, \delta_r, T]$
- the disturbance vector is usually representing the wind velocity, with its six components $D^T = [u_w, v_w, w_w, p_w, q_w, r_w]$

### 2.2.4 Atmospheric Turbulence or Gust

The wind velocity vector may be split into a mean value, considered as constant and horizontal, with coordinates $V_w = [w_n, w_e, 0]^T$ in the earth frame, and a component of atmospheric turbulence (or gust) $V_g = [u_g, v_g, w_g]^T$ and $\Omega_g = [p_g, q_g, r_g]^T$, expressed in the local frame, which may be produced in simulation according to a Dryden model, from three white noise components $n = [n_u, n_v, n_w]^T$.

For simulation purposes, the gust states may be included into the state equation to give a global system as the one simulated in the Matlab function named *fc85.m*.

However, it is often better to keep the modeling of the disturbances as previously, without further detail.

### 2.2.5 Position

The state equation (eq. 11) shows that the aircraft motion only depends on its velocity and attitude (angular position) and the position $P$ of the aircraft c.g. in the earth frame does not appear. If this one is to be monitored, or controlled, it is necessary to introduce position states, as integrators of the aircraft velocity $V$, considered in the earth frame:

$$\dot{P} = S^{-1}V \tag{12}$$

and the three coordinates of $P$ must be added to the previous state vector.

Above equations are used both for the simulation of the aircraft motion and for control design.

## 2.3 Linearized Models

The equations non-linearity, their complexity and a certain level of approximation have justified the search for simplified versions and, as a first step, it is common to linearize the equations for small perturbations around an equilibrium flight. This equilibrium (or trim) flight is frequently taken as a horizontal straight leveled flight, with no wind.

Under these conditions, the equations are written as functions of the perturbations in the state vector $x$, in the input vector $u$ or in the disturbance vector $d$, resulting in two differential matricial equations:

$$\dot{x} = Ax + Bu + Ed \tag{13}$$

describing the dynamics of two independent (decoupled) motions:

- the motion in the vertical plane, named longitudinal, and
- the so-called lateral or lateral/directional motion, mostly in the horizontal plane

The linear dynamic equation may then be written as:

$$\begin{bmatrix} \dot{x}_v \\ \dot{x}_h \end{bmatrix} = \begin{bmatrix} A_v & 0 \\ 0 & A_h \end{bmatrix} \begin{bmatrix} x_v \\ x_h \end{bmatrix} + \begin{bmatrix} B_v & 0 \\ 0 & B_h \end{bmatrix} \begin{bmatrix} u_v \\ u_h \end{bmatrix} + \begin{bmatrix} E_v & 0 \\ 0 & E_h \end{bmatrix} \begin{bmatrix} d_v \\ d_h \end{bmatrix} \tag{14}$$

where the index $v$ is associated with the longitudinal motion (vertical), and the index $h$ is associated with the lateral motion (horizontal).

The linear models described by eq. 14, obviously depend on the trim point chosen for the linearization, namely they are functions of the airspeed $V_o$ and the altitude $h_o$.

The validity of these linear models is obviously limited to a surrounding around the trim point, namely by the linearization of the angles, which cannot exceed an absolute value of say 30 degrees, and by the validity of the aerodynamic laws, which state that the airspeed must be greater than the stall airspeed and lower than the maximum airspeed. The inputs are also limited, both for the surface deflections and for the thrust produced by the propeller.

### 2.3.1 Longitudinal Model

In the deterministic case, with no disturbance, the state vector of the linear longitudinal motion is: $x_v^T = [u, w, q, \theta]$ and the input vector is: $u_v^T = [\delta_e, \delta_T]$ (where all the variables are changes from the trim value).

The approximated longitudinal deterministic dynamics is thus described by the following equation:

$$\dot{x}_v = A_v x_v + B_v u_v \tag{15}$$

or, introducing the matrix components:

$$\begin{bmatrix} \dot{u} \\ \dot{w} \\ \dot{q} \\ \dot{\theta} \end{bmatrix} = \begin{bmatrix} X_u & X_w & 0 & -g \\ Z_u & Z_w & V_o & 0 \\ M_u & M_w & M_q & 0 \\ 0 & 0 & 1 & 0 \end{bmatrix} \begin{bmatrix} u \\ w \\ q \\ \theta \end{bmatrix} + \begin{bmatrix} X_{\delta_e} & X_{\delta_T} \\ Z_{\delta_e} & Z_{\delta_T} \\ M_{\delta_e} & M_{\delta_T} \\ 0 & 0 \end{bmatrix} \begin{bmatrix} \delta_e \\ \delta_T \end{bmatrix} \tag{16}$$

Sometimes the vertical speed $w$ is replaced by the aerodynamic angle of attack: $\alpha \simeq w/V_o$.

### 2.3.2 Lateral Model

In the lateral case, the state vector is: $x_h^T = [v, p, r, \phi]$ and the input vector: $u_h^T = [\delta_a, \delta_r]$.

The dynamic equation:

$$\dot{x}_h = A_h x_h + B_h u_h \tag{17}$$

is then:

$$\begin{bmatrix} \dot{v} \\ \dot{p} \\ \dot{r} \\ \dot{\phi} \end{bmatrix} = \begin{bmatrix} Y_v & 0 & -V_o & g \\ L_v & L_p & L_r & 0 \\ N_v & N_p & N_r & 0 \\ 0 & 1 & 0 & 0 \end{bmatrix} \begin{bmatrix} v \\ p \\ r \\ \phi \end{bmatrix} + \begin{bmatrix} Y_{\delta_a} & Y_{\delta_r} \\ L_{\delta_a} & L_{\delta_r} \\ N_{\delta_a} & N_{\delta_r} \\ 0 & 0 \end{bmatrix} \begin{bmatrix} \delta_a \\ \delta_r \end{bmatrix} \tag{18}$$

Sometimes the lateral speed $v$ is replaced by the side-slip aerodynamic angle $\beta \simeq v/V_o$. The yaw angle $\psi$ appears as a pure integrator of the yaw rate $r$: it may be introduced as an extra state.

### 2.3.3 Model of the X7 UAV

The longitudinal model is computed for a reference (trim) airspeed of 21.9 m/s, near sea level (zero altitude) and is expressed in SI units :

$$\begin{bmatrix} \dot{u} \\ \dot{w} \\ \dot{q} \\ \dot{\theta} \end{bmatrix} = \begin{bmatrix} -0.131 & 0.264 & 0 & -9.81 \\ -1.341 & -3.91 & 21.9 & 0 \\ 0 & -1.59 & -2.74 & 0 \\ 0 & 0 & 1 & 0 \end{bmatrix} \begin{bmatrix} u \\ w \\ q \\ \theta \end{bmatrix} + \begin{bmatrix} 0 & 0.056 \\ 0 & 0 \\ -34.5 & 0 \\ 0 & 0 \end{bmatrix} \begin{bmatrix} \delta_e \\ \delta_T \end{bmatrix}$$

The lateral model for a trim airspeed of 17.9 m/s is:

$$\begin{bmatrix} \dot{v} \\ \dot{p} \\ \dot{r} \\ \dot{\phi} \end{bmatrix} = \begin{bmatrix} -0.169 & 0 & -17.9 & 9.81 \\ -2.409 & -14.48 & 4.874 & 0 \\ 0.835 & -1.16 & -0.893 & 0 \\ 0 & 1 & 0 & 0 \end{bmatrix} \begin{bmatrix} v \\ p \\ r \\ \phi \end{bmatrix} + \begin{bmatrix} 0 & 0 \\ 50.96 & 0 \\ 0 & -15.35 \\ 0 & 0 \end{bmatrix} \begin{bmatrix} \delta_a \\ \delta_r \end{bmatrix}$$

The nominal stall speed is near 12.4 m/s. An airspeed margin of 20 to 30 % is normally needed above the stall speed.

The approximate dynamic model of the ARMOR X7 UAV has been defined in order to enable a realistic simulation, and thus allowing to test control solutions and evaluate strategies for the desired autonomous or semi-autonomous operation.

## 2.4 Flight controller

For the flight control scheme of the UAV ARMOR project ([bri96], [iav98]), a robust control approach is being analyzed.

As is usual in aircraft control, the design of the controllers is based on the linearized decoupled dynamic models, resulting in two complementary controllers, one for the longitudinal motion and one for the lateral, both being in a first step linear and time invariant (LTI).

### 2.4.1 Longitudinal auto-pilot

The longitudinal controller adopted here resulted from a regulator design aimed at tracking of airspeed $V_T$ and altitude $h$:

$$y_{lon} = \begin{bmatrix} V_T \\ h \end{bmatrix}$$

by the use of the elevator deflection angle $\delta_e$ and propeller thrust $T$.

The technique used is a variant of the Loop Transfer Recovery (LTR), with two extra states added to eliminate static errors [iav98].

### 2.4.2 Lateral Controller

The lateral controller is decomposed into a horizontal low-level fast controller, regulating the side slip and roll angles:

$$y_{hll} = \begin{bmatrix} \beta \\ \phi \end{bmatrix}$$

and an outer loop horizontal guidance controller, regulating the horizontal path error, composed of a distance error $d$ and an angular error $\epsilon$:

$$y_{hg} = \begin{bmatrix} d \\ \epsilon \end{bmatrix}$$

The lateral inputs are the aileron and rudder deflection angles, respectively $\delta_a$ and $\delta_r$.

Both low-level and horizontal guidance controllers are designed using a mixed sensitivity $H_\infty$ technique, followed by a robust reduction, resulting in two fifth order discrete controllers.

During the flight phase, the side-slip is normally maintained as low as possible, in order to reduce drag and have a good sensitivity in the path following. However, for the landing phase, banking angles are not desired and the lateral control is based on a side-slip tracking with zero roll demand.

# 3 Image Modeling and Control Objectives

A first step in order to include vision in the control loop is to define a reference scene, the image of which, as viewed from an airborne camera, would allow for a good vertical and lateral or attitude positioning, but leaving freedom enough to cope with the limitations of the landing purpose or the vehicle dynamics.

Let us consider such a landing scene to be a small road or airfield strip, described by three parallel straight lines, the two sides of the road and the center line. The resulting image will have three non-parallel straight lines, the parameters of which depend on the vehicle position and attitude, except for the position along the road axis: the longitudinal speed or position is thus not seen by the image and only the aerodynamics of the vehicle will be used for its control.

According to the landing scene proposed (see figure 1) and depending on the 6D position ($P$) of the airborne camera $C$ in the ground frame, the road appears in the image as 3 straight lines, described by indexes R, C and L, respectively for the right side of the road, the center line and the left side of the road.

The landing scene is defined in the ground NED frame, and the position $P$ of the camera is given by its coordinates in the ABC aircraft frame and by the coordinates and attitude of the aircraft in the NED frame.

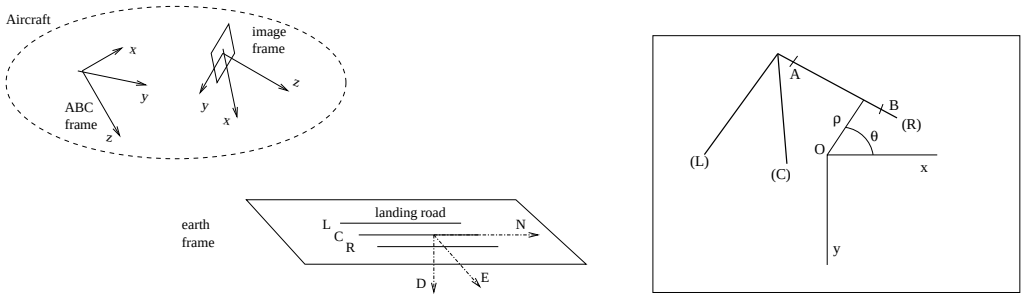


Figure 1: Scene definition (left) and visual output variables in camera image (right)

Without loss of generality the landing road is taken as aligned with the North axis and centered at the origin, giving thus the following lines representation:

$$\begin{cases} D = 0 \\ E = \epsilon_j \frac{L}{2} \end{cases}$$

where $L$ is the width of the landing road, and $\epsilon_j = (+1, 0, -1)$ respectively for the three lines $j = (R, C, L)$.

As represented in figure 1, the 3 lines in the image plane are identified in polar coordinates $(\rho, \theta)$, the definition of which may be found in section 5.1.1.

**Problem statement :** Let us consider the vehicle dynamics as described in a general state space representation by:

$$\dot{x} = f(x, u, d, t) \tag{19}$$

where $x$ is the vector of the relevant state variables describing the vehicle motion, $u$ is the vector of the available control inputs, $d$ is the vector of disturbance inputs, like wind or gust, and $t$ is time.

In order to control the vehicle path, let us define an output equation:

$$y = g(x, u, t) \tag{20}$$

where the output vector includes a subset of state variables $y$, namely with the vehicle absolute position and attitude w.r.t the ground frame, which are the most important variables in the landing phase.

Let us then define the measured variables and image output equation:

$$z = m(y) \tag{21}$$

including the relevant image features $(s)$.

Let then the tracked (desired) vectors be respectively $y^*$ and $z^*$ (a null value in the tracked vector means that an output feedback is used and not an error feedback).

The **position-based visual servoing** approach assumes the output $y$ may be reconstructed or estimated by an inversion of the output equation 21[1]:

$$y = m^{-1}(z) \tag{22}$$

and then a discrete controller is searched for the output error feedback:

$$\begin{array}{c} x^c_{k+1} = A^c_k x^c_k + B^c_k (y^*_k - y_k) \\ u_k = C^c_k x^c_k + D^c_k (y^*_k - y_k) \end{array} \tag{23}$$

where $k$ is the time index and the output error $(y^*_k - y_k)$ is the tracking difference between desired and actual outputs.

The **image-based visual servoing** approach assumes the control objective can be reached by regulating an output function directly expressed in the image. It may be described by a discrete controller for measured output error feedback:

$$\begin{array}{c} x^c_{k+1} = A^c_k x^c_k + B^c_k (z^*_k - z_k) \\ u_k = C^c_k x^c_k + D^c_k (z^*_k - z_k) \end{array} \tag{24}$$

where $k$ is the time index and the output error $(z^*_k - z_k)$ is the tracking difference between desired reference image and actual output image.

# 4 Position-based Visual Servoing

For the position based controller, the image output is considered as an extra sensor with good characteristics to help in the landing phase. The main challenge of this control scheme is to perform a good enough image inversion and pose (position and attitude) reconstruction. The estimated position is then introduced into an adapted version of the normal flight control system.

## 4.1 Image inversion

The basic idea of the reconstruction method is the inversion of the image output 21, in order to retrieve the camera pose, and then the aircraft pose, from the image output.

Following to the definition of the scene and frames presented in figure 1, the three landing straight lines must first be expressed in the image frame and then projected onto the image plane.

The overall transformation from the NED frame to the image frame is the product of:

[1] let us suppose here this inversion or some other state estimation technique is available.

- a rotation and translation from earth frame to local ABC frame
- and a rotation and translation from ABC frame to the image frame.

The second transformation is normally constant and previously known: it would be easily inverted. For a better readability, the camera will be considered here located at the ABC origin, with the optical axis pointing to the aircraft nose. The overall rotation $S_i$ may then be expressed through the Euler angles (roll $\phi$, pitch $\theta$ and yaw $\psi$) by the product of the rotation $S$ from NED to ABC frames, which is given by:

$$S = \begin{bmatrix} 1 & 0 & 0 \\ 0 & \cos\phi & \sin\phi \\ 0 & -\sin\phi & \cos\phi \end{bmatrix} \begin{bmatrix} \cos\theta & 0 & -\sin\theta \\ 0 & 1 & 0 \\ \sin\theta & 0 & \cos\theta \end{bmatrix} \begin{bmatrix} \cos\psi & \sin\psi & 0 \\ -\sin\psi & \cos\psi & 0 \\ 0 & 0 & 1 \end{bmatrix} \tag{25}$$

and a rotation from ABC frame to image frame, corresponding to a rotation of 90° around the z-axis:

$$S_i = \begin{bmatrix} 0 & -1 & 0 \\ 1 & 0 & 0 \\ 0 & 0 & 1 \end{bmatrix} S \tag{26}$$

The position of the lines in the image frame depends on this rotation and on the translation, associated with the aircraft position in the NED frame, with coordinates $(N, E, D)$. Finally, the transformation and then the vision output $(s)$ only depend on the aircraft 6D pose $(P)$.

This image function is obviously neither linear nor bijective, and in particular, as stated above, the longitudinal position $(N)$ along the road cannot be retrieved. An approximate approach is considered here, well adapted to the present case and easier to implement in a real auto-pilot.

As a first step, the rotation $S$ is approximated to a linear form for small angles, corresponding to an aircraft and camera already nearly aligned with the landing field:

$$S \simeq \begin{bmatrix} 1 & -\psi & \theta \\ \psi & 1 & -\phi \\ -\theta & \phi & 1 \end{bmatrix} \tag{27}$$

Then, according to figure 1 and for each line $(y_j = \epsilon_j L/2)$, two points are considered, $P_A = (x, y_j, 0)$ and $P_B = (-x, y_j, 0)$, which are projected in the image plane as 2 points, $A$ and $B$, with coordinates:

$$\overrightarrow{OA} = \frac{f}{c-x} \begin{bmatrix} a - x\psi \\ b + x\theta \end{bmatrix} \qquad \overrightarrow{OB} = \frac{f}{c+x} \begin{bmatrix} a + x\psi \\ b - x\theta \end{bmatrix} \tag{28}$$

where $f$ is the focal length and the parameters $(a, b, c)$ are constant along each line and equal to:

$$\begin{aligned} a &= y_j - E + h\phi \\ b &= -y_j\phi + E\phi + h \\ c &= -y_j\psi + f + (E\psi + h\theta) \end{aligned} \tag{29}$$

But, by definition of the line angle $(\theta_j)$:

$$\frac{\overrightarrow{AB}}{\left\|\overrightarrow{AB}\right\|} = \begin{bmatrix} -\sin\theta_j \\ \cos\theta_j \end{bmatrix} \tag{30}$$

and, analyzing the geometry of triangle $(O, A, B)$, the distance $\rho_j$ may be expressed thru the cross product of vectors $\overrightarrow{OA}$ and $\overrightarrow{AB}$:

$$\rho_j = \frac{\overrightarrow{OA} \times \overrightarrow{AB}}{\left\|\overrightarrow{AB}\right\|} \tag{31}$$

leading thus to:

$$\overrightarrow{OA} \times \begin{bmatrix} -\sin\theta_j \\ \cos\theta_j \end{bmatrix} = \rho_j \tag{32}$$

which, if the abscissa $x$ is great as compared to the other terms, gives the reduced relation:

$$\begin{bmatrix} \psi \\ -\theta \end{bmatrix} \times \begin{bmatrix} -\sin\theta_j \\ \cos\theta_j \end{bmatrix} = \rho_j \tag{33}$$

This relation is obtained for all three lines and results in a matricial expression :

$$\begin{bmatrix} -\sin\theta_R & \cos\theta_R \\ -\sin\theta_C & \cos\theta_C \\ -\sin\theta_L & \cos\theta_L \end{bmatrix} \begin{bmatrix} \theta \\ \psi \end{bmatrix} = \begin{bmatrix} \rho_R \\ \rho_C \\ \rho_L \end{bmatrix} \tag{34}$$

from where the roll and yaw angles $(\theta, \psi)$ may be retrieved:

$$\begin{bmatrix} \theta \\ \psi \end{bmatrix} = \begin{bmatrix} -\sin\theta_R & \cos\theta_R \\ -\sin\theta_C & \cos\theta_C \\ -\sin\theta_L & \cos\theta_L \end{bmatrix}^{\dagger} \begin{bmatrix} \rho_R \\ \rho_C \\ \rho_L \end{bmatrix} \tag{35}$$

with the use of a pseudo-inverse[2].

Once the two angles have been estimated and getting back to the outer product equation (eq. 32), introducing the expressions of parameters $(a, b, c)$ gives:

$$(-x\psi + y_j - E + h\phi)\cos\theta_j + (x\theta - y\phi + E\phi + h)\sin\theta_j = \rho_j\,(f - y_j\psi)\,/f \tag{36}$$

As the above equation must be valid for $x = 0$, and isolating the remaining unknowns $(E, h, \phi)$, yields:

[2] Note that this result is obtained without any further assumptions than the lines being parallel on the ground and the aircraft being almost aligned, with small pitch and yaw angles. Namely, the focal length and the road width are not used.

$$\begin{array}{c}(-\cos\theta_j - \psi\rho_j/f + \phi\sin\theta_j)\,E + (\phi\cos\theta_j + \sin\theta_j - \theta\rho_j/f)\,h + (-y_j\sin\theta_j)\,\phi = \\ -y_j\cos\theta_j + \rho_j - y_j\psi/f\end{array} \quad (37)$$

which, for the three road lines, corresponds to a set of 3 equations with three unknowns. It may be solved by a linear iterative method, assuming initially a zero roll angle ($\phi = 0$), and then obtaining in two or three steps an estimate for the remaining components of the image position: $(E, h, \phi)$.

The output of the image inversion finally gives the estimate of the image frame position resulting from the above process:

$$\overline{P} = [0, \overline{E}, \overline{h}, \overline{\phi}, \overline{\theta}, \overline{\psi}]$$

The process described for the inversion of the image and estimation of the aircraft position has proved to be fairly robust and achieves an accuracy only reduced for roll and East position when the roll angle increases beyond say 5°.

Once the aircraft position has been estimated from the vision output, the aircraft position may also be estimated and the relevant components $(h, d, \epsilon)$ cited above:

$$\begin{cases} \overline{h} \\ d = \overline{E} \\ \epsilon = \overline{\psi} + \beta \end{cases}$$

may be used in the guidance and control of the automatic landing.

## 4.2 Position-based Landing Controller

In section 2.4, the overall output vector used by the flight controller was defined as $y = [V_T, h, \beta, \phi, d, \epsilon]^T$, but from these output variables only a sub-set is likely to be helped by the image output. For the analysis of this implementation method, the output vector was split into:

- low-level flight variables: $y_{ll} = [V_T, \beta, \phi]^T$ to be estimated only from the available flight sensors;
- guidance variables: $y_{gui} = [h, d, \epsilon]^T$ to be estimated from the specific landing sensors, which for the present case consist of the sole camera and its vision output.

The flight auto-pilot is thus implemented according to the reconstruction Block Diagram of figure 2.

Obviously, after touchdown, the auto-pilot is switched from the flight controller to a ground controller, designed to slow down the aircraft while keeping the longitudinal alignment along the road axis.

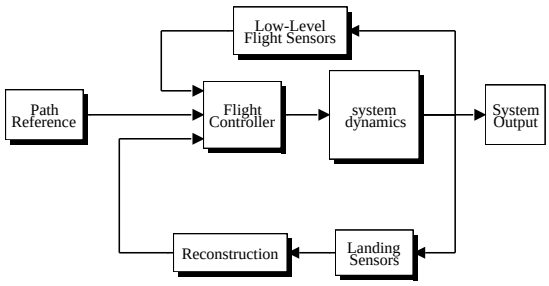


Figure 2: Position-based Control Block Diagram

# 5 Image-based Visual Servoing

In opposite to absolute positioning methods, the image-based visual servoing method does not require an explicit 3D reconstruction of the scene. The basic idea is to assume that a task can be fully specified in terms of the desired configuration of a set of geometric features in the image. The task will be perfectly achieved when such a configuration will be reached [sam90]. In terms of control, this can be formulated as a problem of regulation to zero of a certain output function directly defined in the image frame.

Let us consider the airborne camera $C$ carried by the aircraft which can be viewed as a mechanical system with several actuated degrees of freedom. The pose (position and orientation) of $C$ is an element $\underline{P}$ of $\mathcal{R}^3 \times SO_3$, which is a six dimensional differential manifold. $C$ interacts with its environment. We assume that the image given by $C$ (see figure 1) fully characterizes the relative position of $C$ with respect to the NED frame attached to the scene. Moreover, let us consider that the information in the image may be modeled as a set of *visual signals* characterizing the geometric features which result from the projection onto the image of the 3D objects belonging to the scene. Each elementary signal $s_i(\underline{P})$ defines a differentiable mapping from $\mathcal{R}^3 \times SO_3$ to $\mathcal{R}$. As shown in [esp92], the time derivative of $s_i$ can be expressed by the screw product:

$$\dot{s}_i \doteq \frac{\partial s_i}{\partial t} + H \bullet T_{CT}, \tag{38}$$

where $H$ is called the *interaction screw*, $T_{CT}$ is the velocity screw of the camera and $\bullet$ represents the screw product.

Let us now assume $s$ is a 6-dimensional vector of independent visual signals constructed from the image, then, from equation 38, we can define the image Jacobian (so-called *interaction matrix*) $L^T$ whose rows are interaction screws:

$$\dot{s} \doteq \frac{\partial s}{\partial t} + L^T T_{CT}, \tag{39}$$

An analytical expression for the interaction matrix when the image features are general algebraic curves can be derived (for more details, see [riv96]). In our peculiar case, we consider the set of geometric primitives in the 3D scene is constituted by the three landing straight lines.

## 5.1 Case of staight lines

### 5.1.1 General computation rule for the interaction matrix based on straight lines

Let us consider hereafter both the lines in the 3D scene and their projection in the 2D normalized image plane are expressed in the camera frame $\mathcal{F}_s$.

A straight line in the 3D scene is here represented as the intersection of two planes described in the implicit form $h(\underline{x}, \underline{p}) = 0$ such that :

$$h(\underline{x}, \underline{p}) = \begin{cases} a_1 x + b_1 y + c_1 z = 0 \\ a_2 x + b_2 y + c_2 z + d_2 = 0 \end{cases} \tag{40}$$

with $d_2 \neq 0$ in order to exclude degenerated cases. In these equations, $\underline{x} = (x, y, z, 1)$ denotes the homogeneous coordinates, expressed in the camera frame, of the 3D points lying on the 3D line, and $\underline{p}$ denotes a parameterization of the 3D lines manifold.

The equation of the 2D projected line onto the image plane (see figure 1) can also be written in an implicit form $g(\underline{X}, \underline{P}) = 0$ such that :

$$g(\underline{X}, \underline{P}) = X \cos\theta + Y \sin\theta - \rho = 0 \text{ with } \begin{cases} \cos\theta = a_1 / \sqrt{a_1^2 + b_1^2} \\ \sin\theta = b_1 / \sqrt{a_1^2 + b_1^2} \\ \rho = -c_1 / \sqrt{a_1^2 + b_1^2} \end{cases} \tag{41}$$

where $\underline{X} = (X, Y, 1)$ denotes the homogeneous coordinates expressed in the camera plane, of the 2D points lying on the 2D line, and $\underline{P}$ denotes a parameterization of the 2D lines manifold. In our peculiar case, we have chosen to parameterize the projected 2D line by its polar coordinates $(\rho, \theta)$.

A general form of the interaction matrix may then be obtained for each line:

$$\begin{array}{ll} L_\theta^T = [ & \lambda_\theta \cos\theta \quad \lambda_\theta \sin\theta \quad -\lambda_\theta \rho \quad -\rho \cos\theta \quad -\rho \sin\theta \quad -1 \quad ] \\ L_\rho^T = [ & \lambda_\rho \cos\theta \quad \lambda_\rho \sin\theta \quad -\lambda_\rho \rho \quad (1+\rho^2) \sin\theta \quad -(1+\rho^2) \cos\theta \quad 0 \quad ] \end{array} \tag{42}$$

with $\lambda_\theta = (a_2 \sin\theta - b_2 \cos\theta)/d_2$ and $\lambda_\rho = (a_2 \rho \cos\theta + b_2 \rho \sin\theta + c_2)/d_2$.

In the present case of the automatic landing, we assume that the three 3D lines belong to the ground represented by the plane $P : a_1 x + b_1 y + c_1 z + d_1 = 0$ in the camera frame, and we can select the following 6-dimensional visual signal vector: $s = [\theta_R, \rho_R, \theta_C, \rho_C, \theta_L, \rho_L]^T$, corresponding to the polar coordinates of the right, center and left lines respectively.

The interaction matrix $L^T = \frac{\partial s}{\partial \underline{P}}$ is a $6 \times 6$ matrix but, due to the parallelism between the lines in the scene, it is not full rank: $rank(L^T) = 5$. As previously stated, computing the null space of $L^T$, we find again that only five degrees of freedom are really controlled by the vision data, and the longitudinal motion (along the landing strip axis) is not observable with the only visual output. As this forward speed or the airspeed is responsible for the lift force and thus maintains the aircraft in the air, the airspeed sensor is taken as a landing sensor, along with the visual output.

### 5.1.2 Computing the reference trajectory in the image space

Since a control in the image is used, the path reference to be tracked by the controller is converted into an image reference to be compared with the visual output and then the error is used by the controller. In the visual servoing approach, the control objective is stated as a regulation to zero of an output function fully expressed in the image space. So, we need to translate the Cartesian reference trajectory corresponding to the final approach before landing in terms of image features trajectory.

We assume the Cartesian reference trajectory to be a planar curve defined in the vertical plane which contains the central line of the landing strip ($E = 0$) and parameterized by the camera altitude $h(t)$ and pitch angle $\alpha(t)$ such that $h(t_{start}) = h_0$; $\alpha(t_{start}) = \alpha_0$ and $h(t_{land}) = h_{land}$; $\alpha(t_{land}) = \alpha_{land}$ where $t_{start}$ denotes the beginning of the descent and $t_{land}$ the time of contact with the landing strip (touchdown).

Assuming the distance $L$ between the outer lines of the landing strip is known, we can compute the reference image features as a function of $(h(t), \alpha(t))$:

$$s^*(t) = [\theta_R^*(t)\ \rho_R^*(t)\ \theta_C^*(t)\ \rho_C^*(t)\ \theta_L^*(t)\ \rho_L^*(t)]^T$$

with:

$$\begin{cases} \theta_j^* = \arctan\left[\frac{\epsilon_j L \cos(\alpha)}{2h}\right] \\ \rho_j^* = \frac{-\epsilon_j f L \sin(\alpha)}{\sqrt{4h^2 + L^2\cos^2(\alpha)}} \end{cases} \tag{43}$$

where $f$ is the focal length of the camera and, for $(j = R, C, L)$, $\epsilon_j$ is respectively given by $(+1, 0, -1)$.

Alternatively, the reference trajectory may more conveniently be stated in terms of distance to touchdown, here equal to $N$, instead of a time function, giving a parameterization by the camera altitude $h(N)$ and pitch $\alpha(N)$, and a reference image $s^*(N)$. Clearly, the choice for an altitude profile $h(N)$ implies the use of an extra longitudinal position sensor, which might be a GPS receiver by instance, and which was taken as an ideal sensor in the following exploratory simulations.

## 5.2 Image-based Landing Controller

The image-based auto-pilot is thus implemented according to the Block Diagram of figure 3, with the use of an airspeed sensor and a camera as only landing sensors, and with a specific controller regulating the airspeed error and tracking the image reference constructed as above.

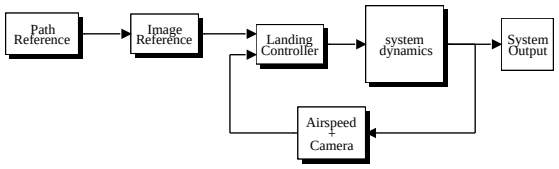


Figure 3: Image-based Control Block Diagram

### 5.2.1 Controller Design

The idea of a visual control for an unstable platform of 12th order is challenging but implies a great concern with the robustness of the solution.

As a first tentative, a solution is searched using optimal control, based on the linearized model of the vehicle motion and image output (equations 14 and 21), looking for a pure gain applied on the measured output error:

$$u_k = D_k \left( z_k^* - z_k \right) \tag{44}$$

where the output $z = [u, \theta_R, \rho_R, \theta_C, \rho_C, \theta_L, \rho_L]^T$ includes the longitudinal speed $u$ and the visual output $s$, in order to allow for the observability and control of the full vehicle position.

The non-linear dynamics of the air vehicle is first linearized using the classical techniques of flight mechanics, and a state space model is obtained around a trim equilibrium state corresponding to a stabilized leveled flight at a constant airspeed ($V_o$) and at a constant altitude ($h_o$) above the landing road and aligned with the road axis:

$$\dot{X} = A\left(V_o\right) X + B\left(V_o\right) U$$

The state $X = [u, v, w, p, q, r, n, e, d, \phi, \theta, \psi]^T$ of this model includes the 6D change in velocity $\mathbf{v} = [u, v, w, p, q, r]^T$ and 6D change in position $\mathbf{p} = [n, e, d, \phi, \theta, \psi]^T$ of the aircraft and camera frames with respect to the ground frame. The input ($U$) includes the 3 control surface deflections ($\delta_a, \delta_e, \delta_r$) and the engine thrust changes ($\delta_T$).

The visual output is also linearized, for the same trim condition, using the Jacobian of the image function (or interaction matrix 42) and including the change from aircraft ABC frame to image frame ($S_a$):

$$s = L^T(h_o) S_a \mathbf{p}$$

which, together with the longitudinal speed change $(u)$, gives the output equation:

$$Z = C\,(V_o, h_o)\, X = \begin{bmatrix} C^u & 0 \\ 0 & L^T S_a \end{bmatrix} \begin{bmatrix} \mathbf{v} \\ \mathbf{p} \end{bmatrix} \tag{45}$$

where $C^u = [1, 0, 0, 0, 0, 0]$ extracts the first velocity component.

For a fixed airspeed and altitude, the optimal state feedback gain of the LTI system is obtained with the Matlab *lqr* function corresponding to the minimization of a cost function weighting the output error and control needs:

$$J = \int_0^\infty \left( Z^T Q Z + U^T R U \right) dt \tag{46}$$

through the definition of the appropriate weighting matrices $Q$ and $R$.

The state feedback gain $K$ is finally transformed into an output error feedback gain using the pseudo-inverse of the output matrix[3]:

$$D = K C^{-1} \tag{47}$$

### 5.2.2 PI controller

In order to cancel the static error appearing in the previous solution in the case of a constant wind disturbance, an error integrator $Z_i$ was added in the previous procedure:

$$\begin{bmatrix} \dot{X} \\ \dot{Z}_i \end{bmatrix} = \begin{bmatrix} A & 0 \\ C & 0 \end{bmatrix} \begin{bmatrix} X \\ Z_i \end{bmatrix} + \begin{bmatrix} B \\ 0 \end{bmatrix} U$$
$$Y = \begin{bmatrix} C & 0 \\ 0 & I \end{bmatrix} \begin{bmatrix} X \\ Z_i \end{bmatrix} \tag{48}$$

The resulting optimal state feedback gain was converted into an output error feedback and then the PI discrete controller was deduced:

$$\begin{aligned} x^c_{k+1} &= A^c x^c_k + B^c \left( z^*_k - z_k \right) \\ u_k &= C^c x^c_k + D^c \left( z^*_k - z_k \right) \end{aligned} \tag{49}$$

[3] An alternative direct computation of the optimal output error feedback was also used, with very similar results.

### 5.2.3 Sliding Gain

In order to cope with the change in the linearized system as altitude is changing, and namely because the Jacobian of the image is increasing dramatically when the vehicle is near touchdown, the interaction matrix is computed at each sample time according to the current altitude and the applied feedback gain is updated:

$$u_k = C_k^c x_k^c + D_k^c (z_k^* - z_k) \tag{50}$$

The weighting matrices are also updated as altitude reduces in order to integrate the strict constraints near touchdown.

Obviously, here again, the visual control is only valid in flight and is switched off once the aircraft has landed and is rolling on the ground (the case is exactly the same for the position-based visual servoing scheme).

# 6 Simulation Results

In order to allow for a fair comparison, a similar setup was used for both simulations, in agreement with the Block Diagrams presented above. However, the flight controller used in the position-based scheme is a LTI controller previously designed for the normal flight control, and is used here during the landing phase whereas the image-based controller is designed specifically for the landing purpose. One consequence of this is that the sampling rate used by the normal flight controller is kept to the flight value at 100ms (10Hz), while the image processing and image-based control is computed at a sampling period of 40ms (25Hz).

The following landing conditions were assumed:

- start at $700m$ away from the touchdown point on the road; after a stabilization period, the landing control was switched on at $500m$ from the desired touchdown, with alignment first and then descent;
- initial altitude at $20m$ reference;
- initial airspeed at reference speed, equal to $16m/s$, which corresponds to an airspeed adequate for the approach phase, with a pitch attitude acceptable until touchdown (the model stall speed is slightly below $13m/s$ ).

Two altitude profiles were first considered:

- an usual linear descent at constant sinking speed, with a glide slope of 3 degrees, and flare for touchdown, with a final reduction of airspeed before ground contact;
- a cosine descent, varying continuously from the initial altitude to touchdown, with also an airspeed reduction for ground contact.

Both profiles were analyzed in the longitudinal nominal case, and then the cosine profile was used.

The simulation results presented here are organized for a step-by-step comparison of the two visual control schemes:

1. longitudinal nominal, with a flight path in the vertical plane, no disturbance: here two sub-cases are devoted to the comparison between the linear and cosine profiles;
2. lateral nominal, without any descent phase and only the correction of an initial lateral error of $5m$;
3. landing nominal, with lateral correction and descent to touchdown, without disturbances;
4. landing with constant wind and gust disturbances.

All the curves have as abscissa the longitudinal distance to pretended touchdown along the road $(N)$, corresponding to simulations with around 55 seconds of flight. References are presented in dashed curves, simulation output under visual control in solid and before or after visual control in dotted curves.

## 6.1 Longitudinal nominal behavior

### 6.1.1 Linear descent

Here is presented a nominal landing, in no wind, no lateral error, with descent along a linear profile from a stabilized flight at $20m$ of altitude, aligned with the road axis, down to touchdown.

The simulation results are shown in figure 4, with the image-based case on the left and the position-based case on the right. From top to bottom are presented the altitude and airspeed curves, along with their reference profiles, the pitch angle and the two longitudinal inputs, thrust demand and elevator deflection.

The altitude profiles demonstrate a fair tracking of the reference, with a little lag at the start of descent, smoothly corrected for both above $12m$. The airspeed profile exhibit the influence of the descent on the airspeed regulation, but the reference airspeed is still well tracked.

Both the flare in the altitude profiles and the airspeed curves seem to be more precise in the image based case.

The pitch curves are more contrasting: the position-based curve exhibits a different flare behavior and a more noisy second part. These two aspects are present in the input curves: namely, the elevator curve appears as somewhat noisy.

The aspect of the image output (here the angle and distance for the right line) are shown in figure 5. The curves are very similar in the first part of the descent, only the flare zone seems to be different.

The altitude estimation from the image inversion (fig. 6) appears as quite good, with no visible error between the dashed line (estimated altitude) and solid line (actual altitude). The lateral error estimation is negligible in magnitude terms and the noise component appearing may not be related to the noisy pitch angle. Indeed, the longitudinal noise is due to the lower rate used in the flight longitudinal controller, but the amplitude of this noise, only visible in the steepest part of the descent, was considered as acceptable in this exploratory evaluation work.

In terms of airplane automatic landing, the performance of this nominal case may be analyzed thru the impact vertical velocity (sinking speed) as presented in figure 7, which is to be compared to the regulation limit of $2m/s$[sbac91]. Both solutions are well inside the regulation limits, but here again the image-based solution seems to be better, with an impact velocity near 0.4m/s, while the other one exhibits a value over 0.8m/s.

### 6.1.2 Cosine descent

Here is presented a nominal landing again, in no wind, no lateral error, but now with a descent along a cosine profile from a stabilized flight at $20m$ of altitude down to touchdown.

The simulation results are shown in figure 8, with the image-based case on the left and the position-based case on the right. From top to bottom are presented the altitude and airspeed curves, along with their reference profiles, the pitch angle and the two longitudinal inputs, thrust demand and elevator deflection.

The altitude profiles demonstrate again a fair tracking of the reference. However, the lag at the start of descent is still smoothly corrected for the image-based case and then the reference is perfectly tracked, whereas the position-based curve also presents a small lag during the flare phase. The airspeed profiles exhibit the influence of the descent on the airspeed regulation, but with a tighter control in the image-based case.

The flare in the altitude profile is more precise in the image based case, the airspeed profile is more precise in the other case.

The pitch curves for this cosine descent are more consistent, even though some noise is seen in the steepest part of the descent. These two aspects are present in the input curves: namely, the elevator curve appears as a little noisy again.

The aspect of the image output (here the angle and distance for the right line) are shown in figure 9. The curves are very similar in the first part of the descent, only the flare zone seems to be different and some noise is again visible in the position-based $\rho_R$ curve.

The altitude estimation from the image inversion (fig. 6) appears as quite good, with a very little error between the dashed line (estimated altitude) and solid line (actual altitude). The lateral error estimation is again negligible in magnitude terms.

In terms of airplane automatic landing, the performance of the impact vertical velocity is presented in figure 11. Both solutions are well inside the regulation limits, but with this

cosine descent, the impact velocity is below 0.4m/s for both solutions, maybe with a more smooth curve in the image-based case.

>From the comparison of the longitudinal landing performances with linear and cosine descents, it was decided to perform the remaining simulations with cosine descents only, due to the more continuous curves it implied and to the reduced impact velocity.

## 6.2 Lateral nominal behavior

Here is presented a nominal lateral simulation, in no wind, at a constant reference altitude, at $20m$, with an initial lateral error of $5m$ to the right of the landing road.

The simulation results are shown in figure 12, with the image-based case on the left and the position-based case on the right. From top to bottom are presented the lateral position error and yaw error angle, the two lateral inputs, aileron and rudder deflections. Both solutions take the aircraft back to the road axis before the desired landing point, but, in terms of comparison, two conclusions may be drawn from these figures:

- a huge position overshoot, near $5m$ or a 100%, is exhibited by the image-based solution whereas the position based solution has less than $1.5m$ overshoot;
- the damping of the image-based solution is far better and the position-based remains oscillating almost till the end of the simulation.

Probably, both characteristics are due to the input options implied by the two control schemes:

- in order to ensure a fair image inversion, the position based solution uses a control based on side-slip manoeuvres, with a zero roll reference position: the aileron and rudder inputs are both used for the trajectory correction, but the control quality is reduced if compared to the normal flight lateral control, mostly based on aileron inputs and no side-slip;
- the image-based solution implies no inversion and is nearly not using the rudder input, but the rolling motion is such that the decoupling between lateral and longitudinal motions does not strictly apply any longer.

This explanation of the lateral behavior may be further demonstrated with the longitudinal response to this lateral correction as presented in figure 13. The airspeed curves show that both controls perform a good regulation but in terms of altitude, the image-based solution induces a loss of $2m$, whereas for the other one the loss is less than half.

The aspect of the right line image outputs are shown in figure 14. The contrast between the two control schemes is here again obvious, with the high angular overshoot in the image-based case and the low damping in the other case.

The lateral error estimation from the image inversion (fig. 15, right) exhibits an exaggerated oscillation, up to a maximum of 2m, which certainly does not help to stabilize the

motion in the position-based scheme. The altitude estimation error (left curve) is comparatively small.

## 6.3 Nominal landing

This is the simulation of a nominal landing from $20m$ down to touchdown, with a cosine descent and with an initial lateral error of $5m$, without any wind. The results are presented in figure 16.

To some extent the characteristics of both control schemes are in agreement with the pure longitudinal and lateral cases. In the case of the position-based scheme however the descent seems to stabilize the lateral motion, the oscillations are quickly reduced and only a small lateral error of $10cm$ remains at touchdown.

The image output for these simulations are presented in figure 17. In a first phase, during the lateral alignment, the image-based control hardly seems to be tracking the reference image but then the angle $\theta_R$ seems to behave quite well, even though it is less obvious for the distance $\rho_R$ case.

The image estimation for the position-based control (figure 18) is in agreement with the previous cases, a good altitude and an over-oscillating lateral error.

## 6.4 Landing in wind and gust

In order to have a first evaluation of the disturbance robustness of the two control schemes, a windy landing simulation was run, from $20m$ down to touchdown, with a cosine descent and with an initial lateral error of $5m$ to the right of the road. The wind conditions were defined with:

- a mean nose component with $5m/s$, with a 10 degrees angle to the right of the landing road (the wind intensity corresponds to 31% of the aircraft airspeed, regulated to $16m/s$, and is quite significative);
- plus an atmospheric turbulence component simulated by a Dryden model with an intensity of $3m/s$, which, in a scale from 0 to $7m/s$, corresponds to a intermediate gust case.

The simulation results are presented in figure 19. The comparison with the nominal no-wind case is quite satisfactory, the altitude and airspeed references are fairly tracked, and the correct landing is ensured for both cases, with an impact vertical speed (bottom curves) below $0.4m/s$. The effects of the wind and gust disturbances are however obvious:

- the right wing wind results in a high lateral overshoot to the left of the road (up to $8m$ for the image-based scheme and less than $4m$ for the position-based control);
- the gust input is visible in the airspeed curve, but the most affected seems to be the position-based sinking speed, with a low damped oscillation.

The image output for these windy simulations are presented in figure 20. When compared with the no-wind case, the disturbance effect seems quite reduced and the image features exhibit a global behavior in agreement with the deterministic cases.

The image estimation for the position-based control (figure 21) is also in agreement with the previous cases, showing a good altitude and an over-oscillating lateral error.

# 7 Conclusions

In the work described in this report, two control schemes have been analyzed in order to set a first exploratory evaluation of a visual servoing technique applied to the automatic landing of a unmanned aircraft (UAV).

The two classical approaches, defined as position-based and image-based, were adapted to the specific case:

- an adequate scene and image features were selected to allow for the proposed objective;
- in the position-based control, an image inversion was setup and its position estimate was used in the pre-existing flight control scheme;
- in the image-based control, the design had to include the aircraft dynamic characteristics and a sliding gain optimal control was chosen as a first robust solution.

In terms of comparison between the two visual control schemes, despite the quite consistent results, the contrast is obvious:

- the position-based or reconstruction approach is based on robust control methods and is using a set of two low-level controllers plus a guidance controller, each of them with 5 internal states, building up a total of 15 states; whereas the image-based approach is here using a simple proportional plus integral feedback gain, produced in an optimal output feedback design, corresponding to an internal dynamics with 7 (error integrator) states;
- the position-based approach needs the computation of the image inversion, whereas the image-based only computes image features errors: a better robustness is thus available;
- the robustness of the flight control and reconstruction solution allows to keep a constant LTI controller down to the ground; the image inversion is depending on a good calibration but then its solution covers a wide range in admissible positions and attitude;
- during the alignment and mostly in the descent, as altitude comes near zero, the image reference very rapidly changes and the image-based solution needs a sliding gain scheme to adapt the control as the aircraft is descending to touchdown: the image-based design is a function of the altitude and the optimal controller must be computed on-line;

- as for the lateral error, the convergence zone, where the error feedback leads to a stable regulation, is smaller for the image-based scheme than for the image inversion: even though the lateral error estimate is polluted by the rolling of the aircraft, the quality of the lateral reconstruction control is independent of the altitude.

The simulations used to analyze the close loop characteristics and the behavior of both control solutions permitted to verify a fair performance, in agreement with the specifications, and both schemes were able to land the aircraft in nominal and intermediate wind conditions. The idea seems feasible but clearly further studies should be performed before any of such schemes may be implemented on the real aircraft.

# References

[cos99] Costa, N., *Modelação da Aeronave Robotizada ARMOR X7*, IST, 1999

[mcl90] McLean, D., *Automatic Flight Control Systems,* Prentice-Hall, 1990.

[mcc95] McCormick, B.W., *Aerodynamics, Aeronautics and Flight Mechanics,* John Wiley & Sons, 1995.

[ste92] Stevens, B.L. and Lewis, F.L., *Aircraft Control and Simulation,* John Wiley & Sons, 1992.

[bri96] J.R.Azinheira, P.M.Lourtie, J.P.Rente, "Robust Control and Guidance for a Low Cost Civilian RPV", XIIth Int.Conf. on RPV's, Bristol, UK, 1996

[iav98] J.R.Azinheira, J.P.Rente, M.G.Kellett, "Longitudinal Auto-Landing for a Low Cost UAV", IAV'98, Madrid, Spain, 1998

[esp92] B. Espiau and F. Chaumette and P. Rives, "A New Approach to Visual Servoing in Robotics", IEEE Transactions on Robotics and Automation, Vol.8, N.3, June 1992.

[riv93] P. Rives and H. Michel, "Visual Servoing based on Ellipse Features", SPIE, Boston, MA, USA, September 1993.

[riv96] P. Rives and R. Pissard-Gibollet and L. Pelletier, "Sensor-based Tasks: From the Specification to the Control Aspects", 6th Int. Symposium on Robotics and Manufacturing (WAC), Montpellier, France, May 28 - 30, 1996.

[riv97] P. Rives and J.J Borrelly, "Underwater Pipe Inspection Task using Visual Servoing Techniques" Int. Conf. on Intelligent Robots and Systems, IROS, Grenoble, France, September 8-12, 1997.

[sam90] C. Samson, B. Espiau, M. Le Borgne : *Robot control: the task function approach*, Oxford University Press, 1990.

[sbac91] SBAC Guided Weapons Ranges Commitee, "Unmanned Air Vehicles: Guide to the Procurement, Design and Operation of UAV Systems", UK, 1991

[chat98] G.B. Chatterji, P.K. Menon, B. Sridhar, "Vision based Position and Attitude Determination for Aircraft Night Landing", Journal of Guidance, Control and Dynamics, Vol 21, No 1, pp 84-91, 1998

[kimm02] J. Kimmett, J. Valasek, J.L. Junkins, "Vision Based Navigation SSSystem for Autonomous Aerial Refueling", Conf. on Control Applications, CCA 2002, Glasgow, pp1138-1143, Sep 2002

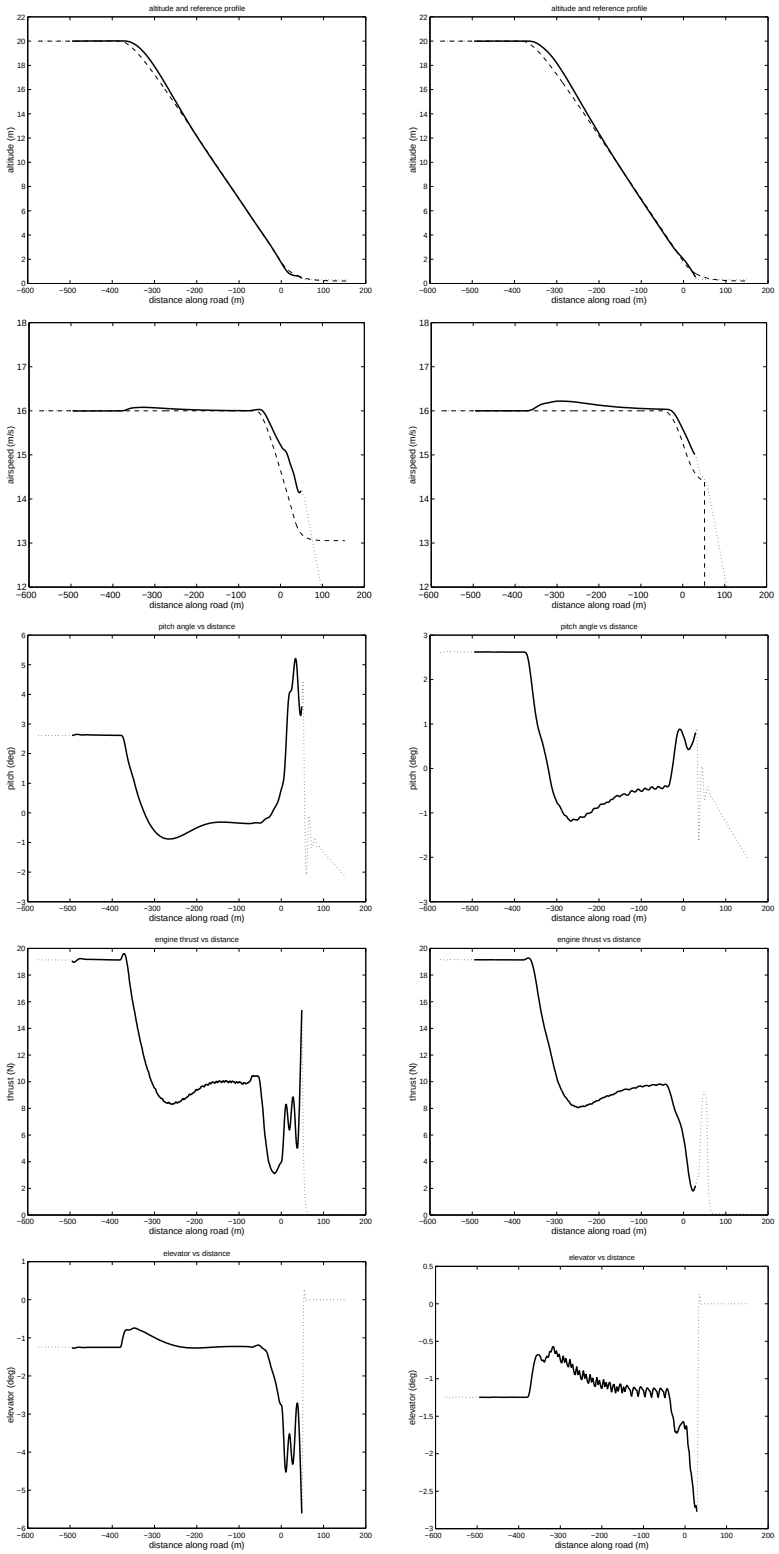




Figure 4: Longitudinal nominal in linear descent, with image-based (left) and position-based (right) control schemes, with from top to bottom the altitude profiles, airspeed, pitch angle, thrust demand and elevator deflection.

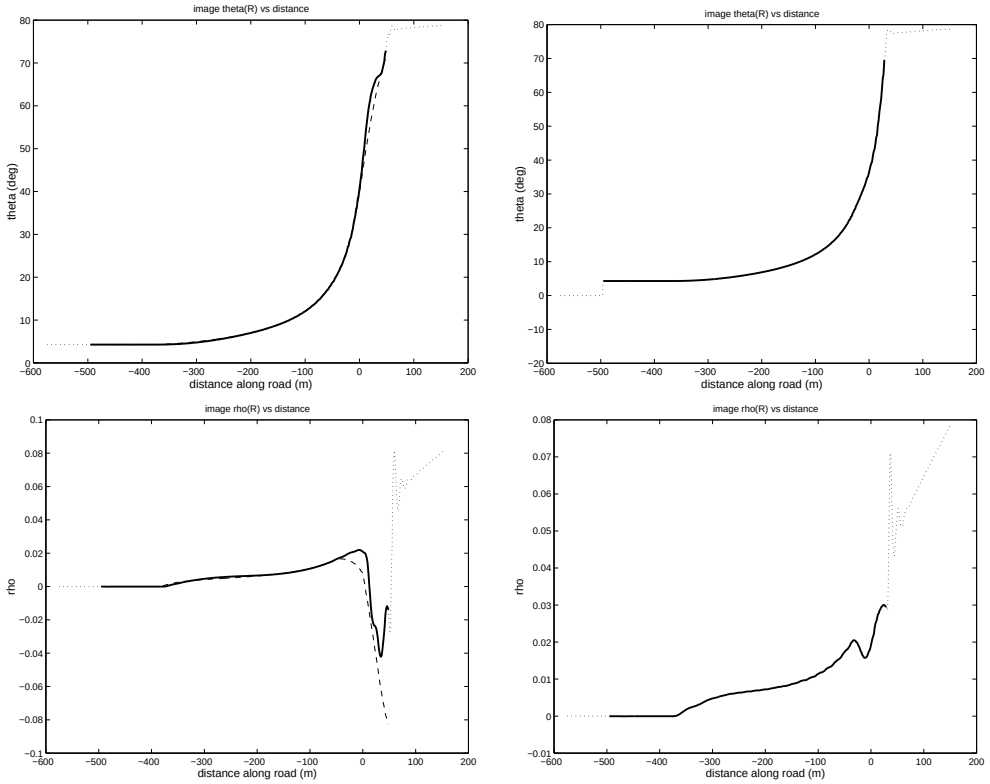


Figure 5: Longitudinal nominal in linear descent, with image-based (left) and position-based (right) control schemes, with $\theta_R$ on top and $\rho_R$ bottom.

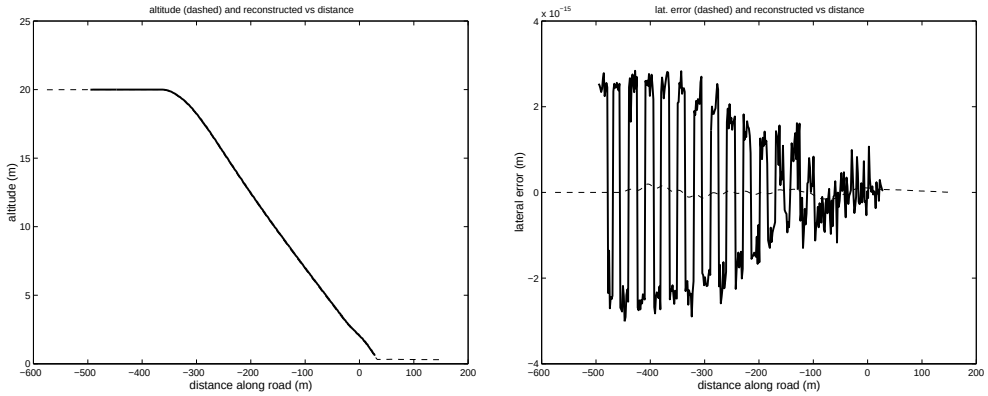


Figure 6: Longitudinal nominal linear descent, image inversion: altitude (left) and lateral error (right) estimation

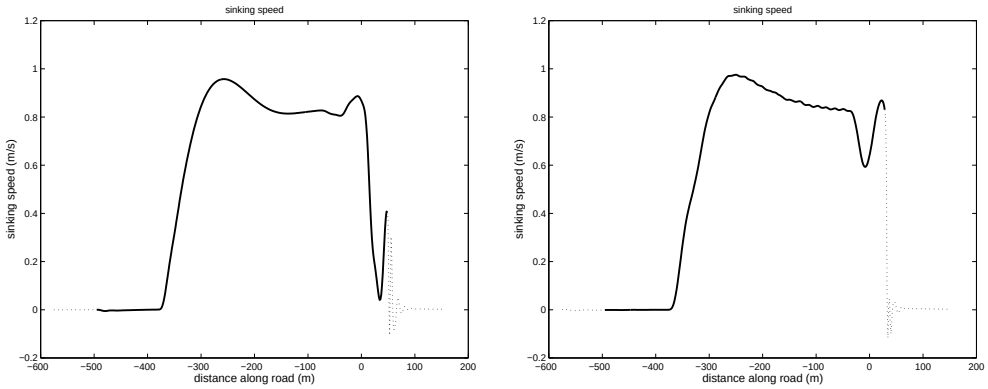


Figure 7: Sinking speed for image-based (left) and position-based (right) control schemes

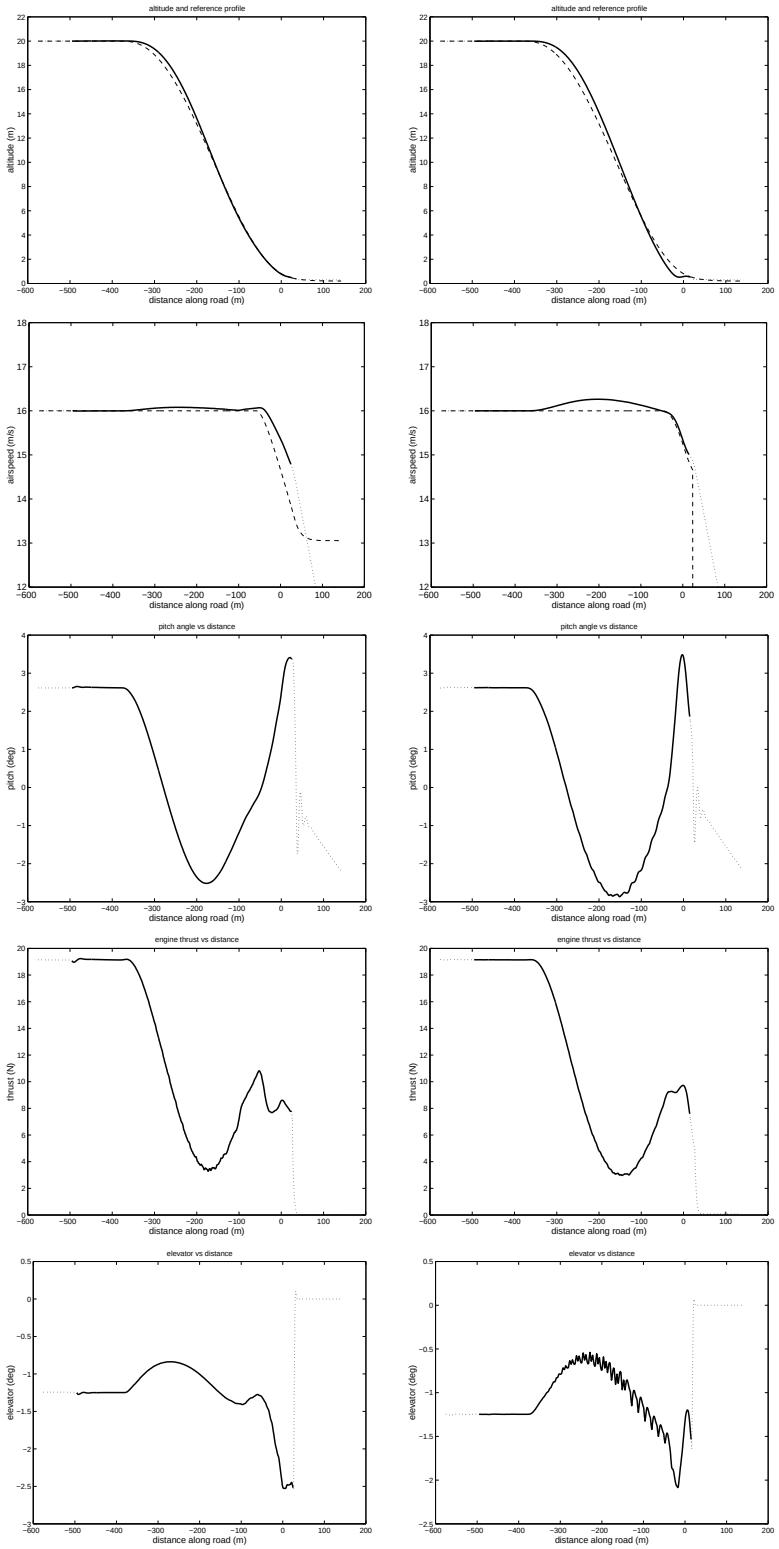




Figure 8: Longitudinal nominal in cosine descent, with image-based (left) and position-based (right) control schemes, with from top to bottom the altitude profiles, airspeed, pitch angle, thrust demand and elevator deflection.

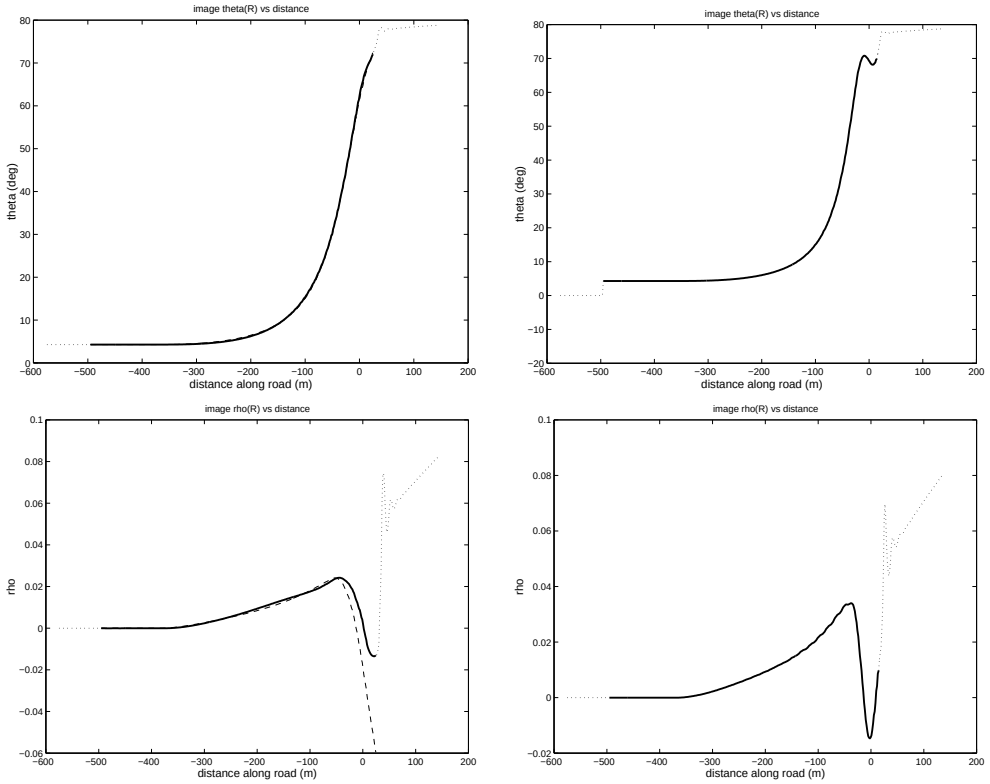


Figure 9: Longitudinal nominal in linear descent, with image-based (left) and position-based (right) control schemes, with $\theta_R$ on top and $\rho_R$ bottom.

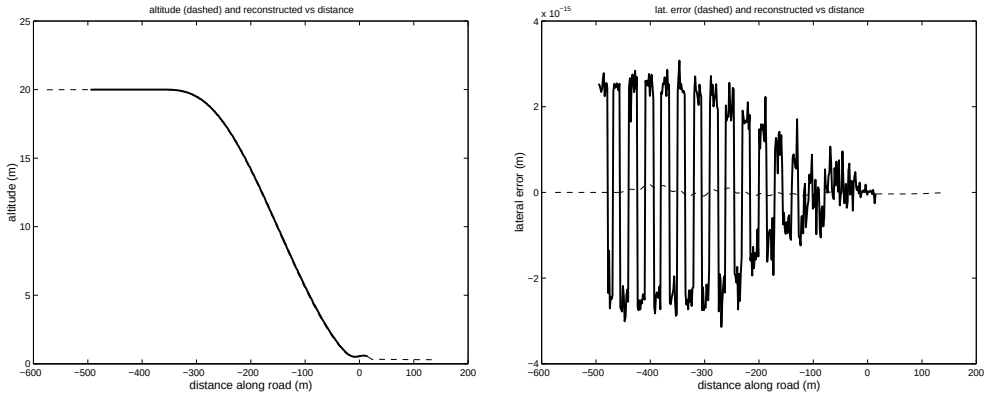


Figure 10: Longitudinal nominal linear descent, image inversion: altitude (left) and lateral error (right) estimation

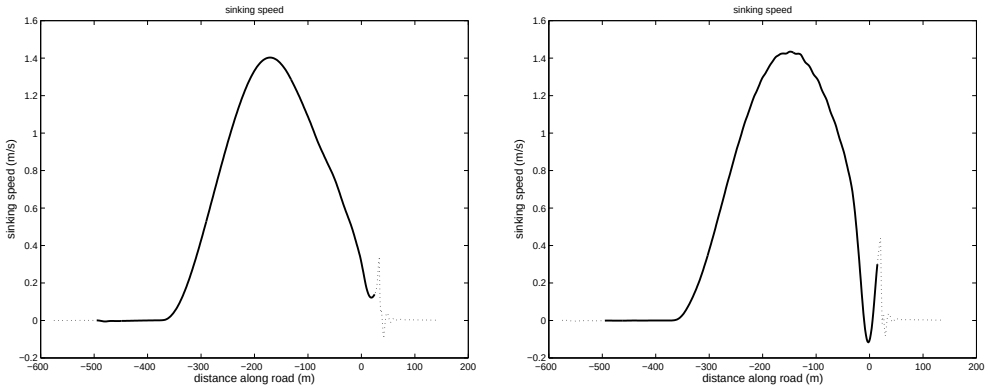


Figure 11: Sinking speed for image-based (left) and position-based (right) control schemes

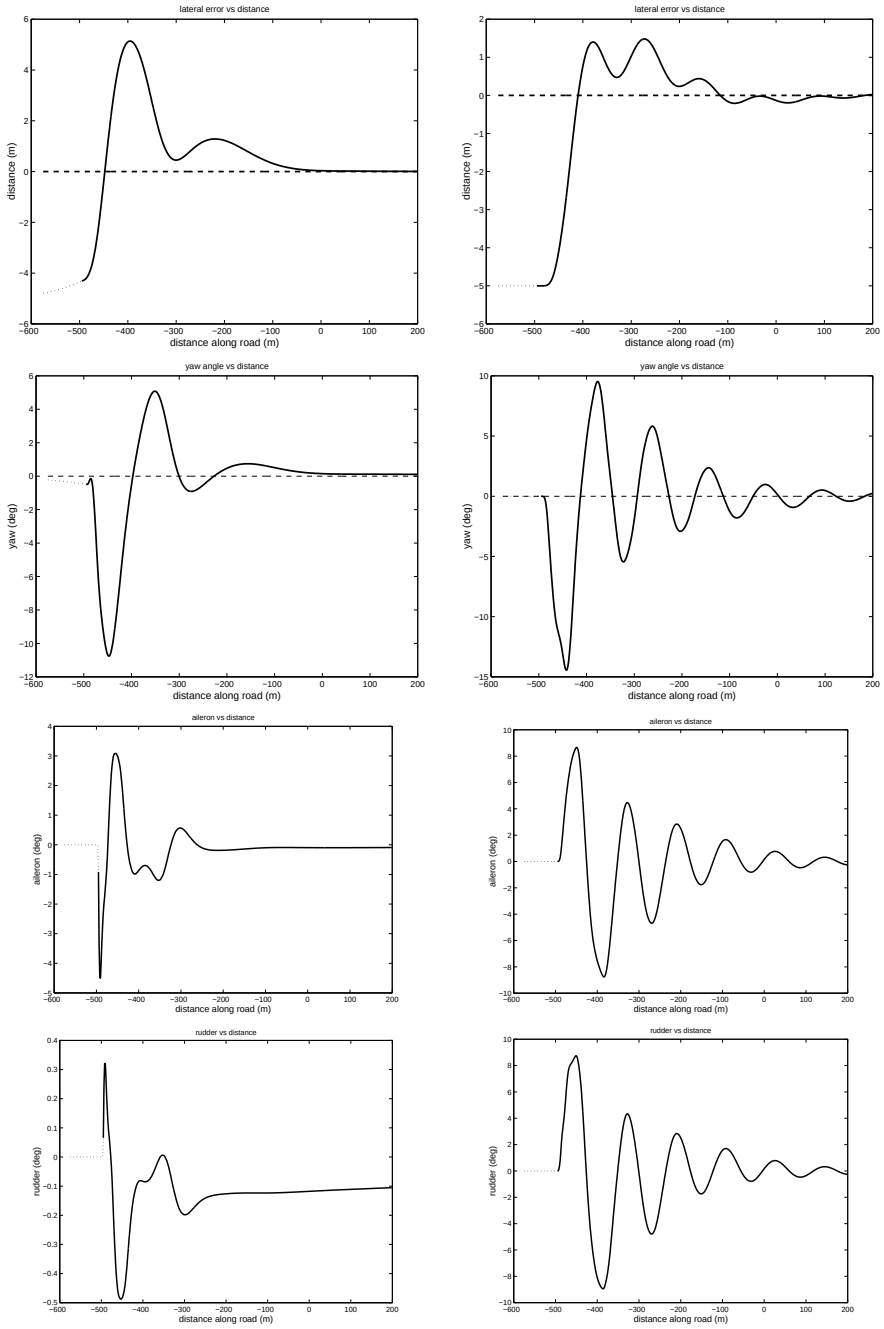


Figure 12: Lateral behavior results with image-based (left) and position-based (right) control schemes: form top to bottom, lateral error, yaw error, aileron and rudder deflections.

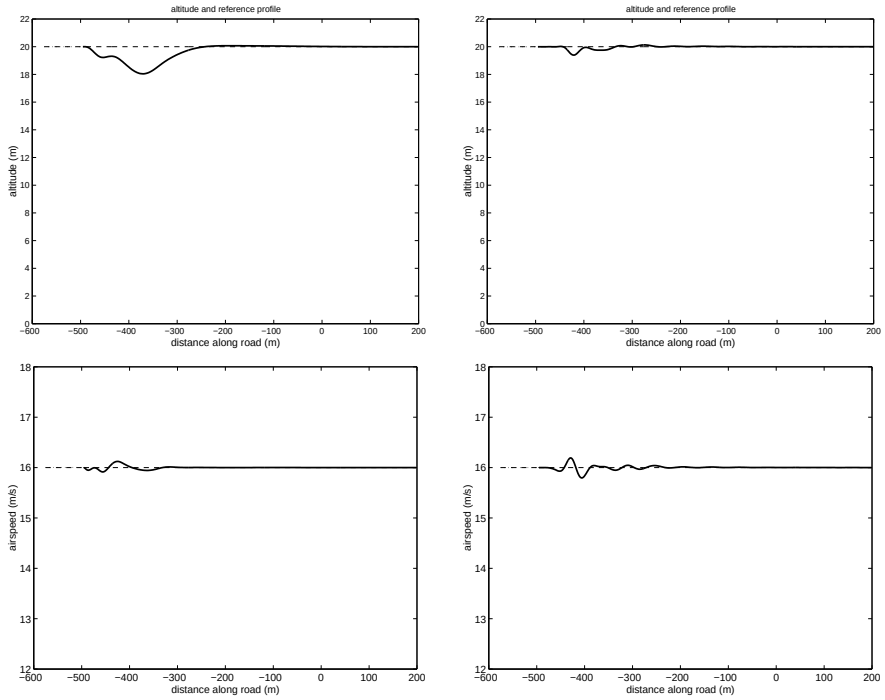


Figure 13: Lateral to longitudinal coupling, with image-based (left) and position-based (right) control schemes, with from top to bottom the altitude and airspeed curves.

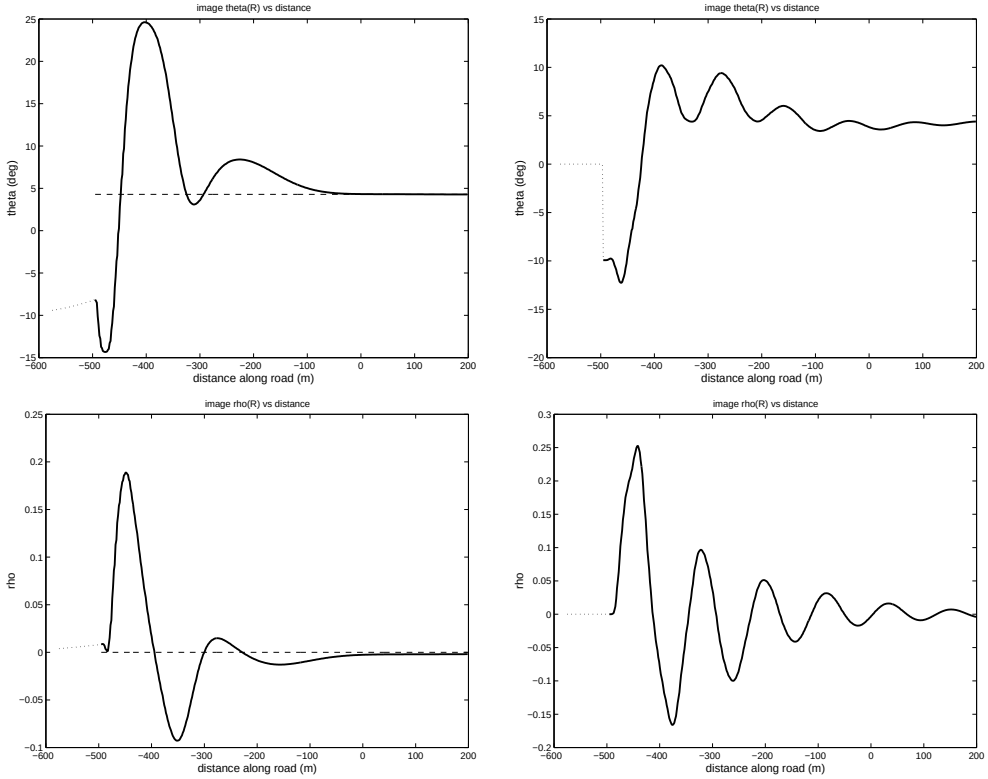


Figure 14: Lateral behavior, with image-based (left) and position-based (right) control schemes, with $\theta_R$ on top and $\rho_R$ bottom.

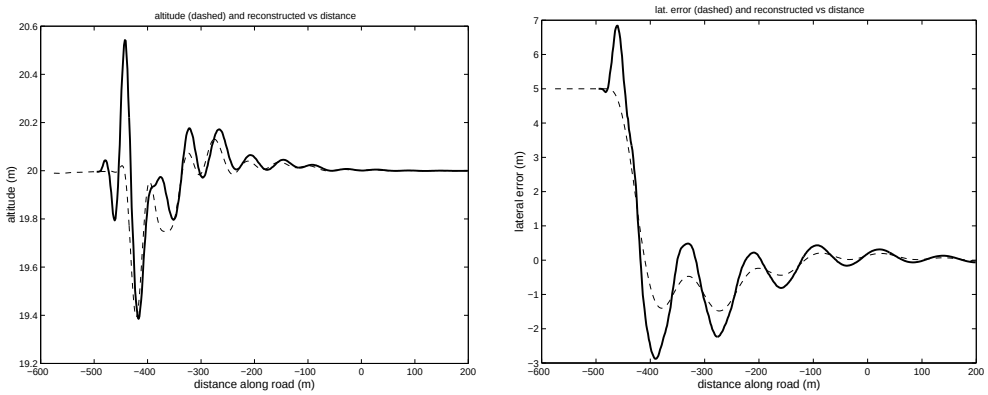


Figure 15: Image inversion in lateral response: altitude (left) and lateral error (right) estimation

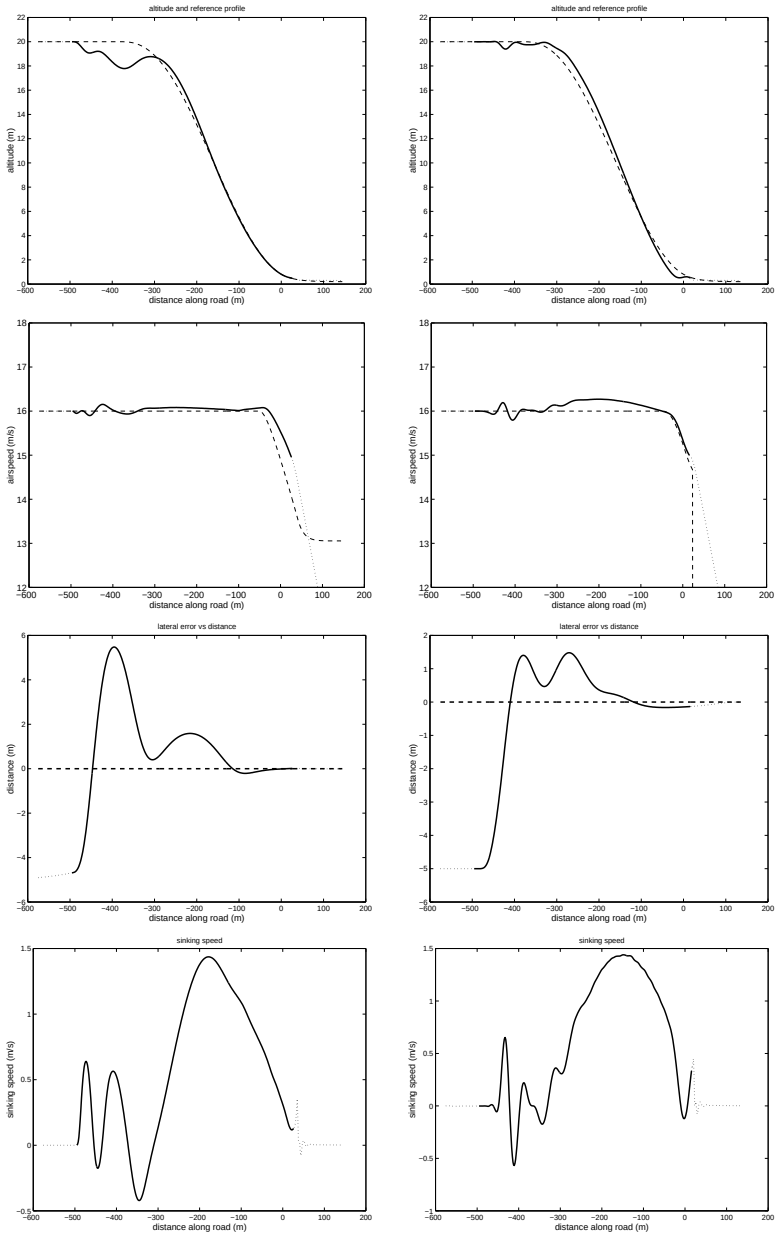


Figure 16: Nominal landing results with image-based (left) and position-based (right) control schemes: form top to bottom, altitude, airspeed, lateral error and sinking speed.

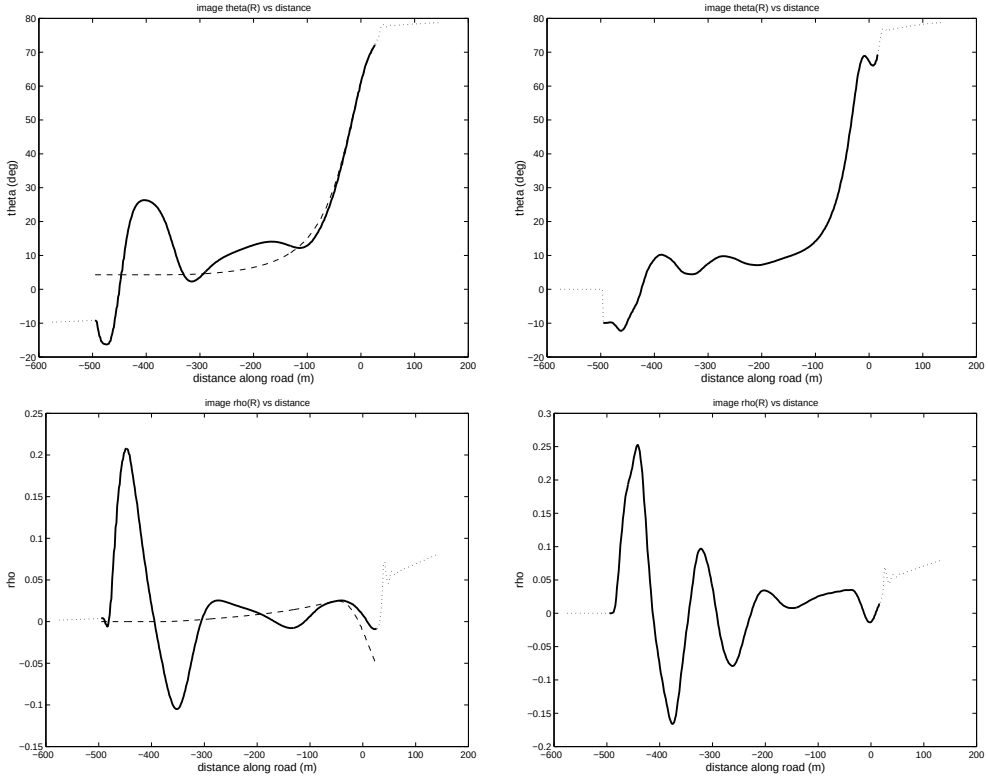


Figure 17: Nominal landing image outputs, for image-based (left))) and position-based (right) schemes, with $\theta_R$ on top and $\rho_R$ bottom.

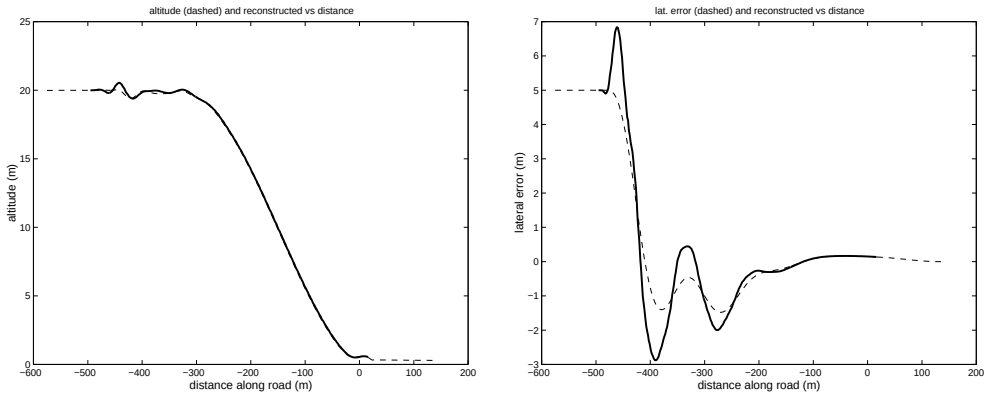


Figure 18: Nominal landing image estimation, with altitude (left) and lateral error (right) compared with real values in dashed.

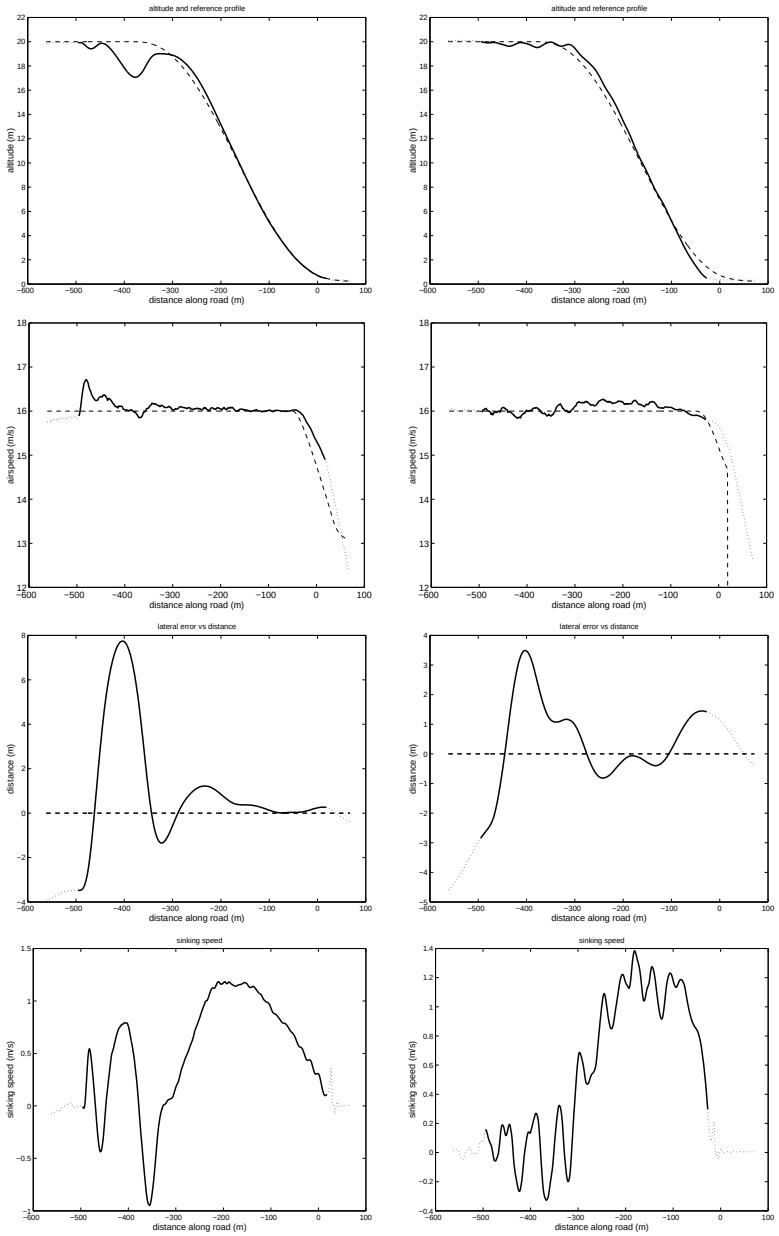


Figure 19: Windy landing results with image-based (left) and position-based (right) control schemes: form top to bottom, altitude, airspeed, lateral error and sinking speed.

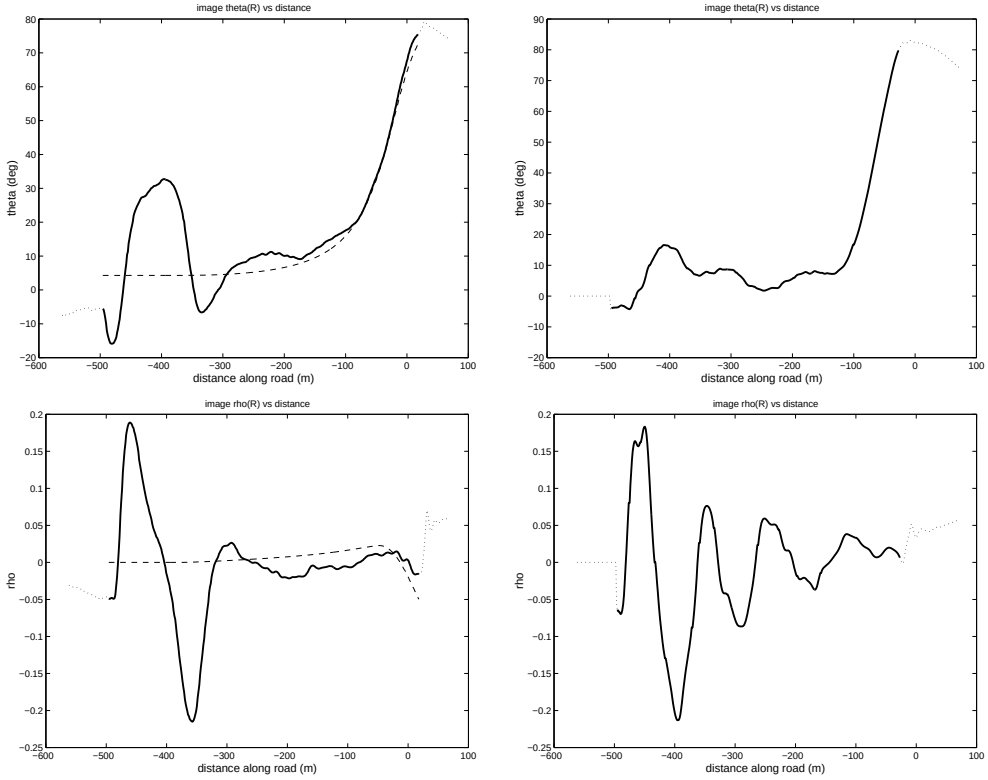


Figure 20: Windy landing image outputs, for image-based (left))) and position-based (right) schemes, with $\theta_R$ on top and $\rho_R$ bottom.

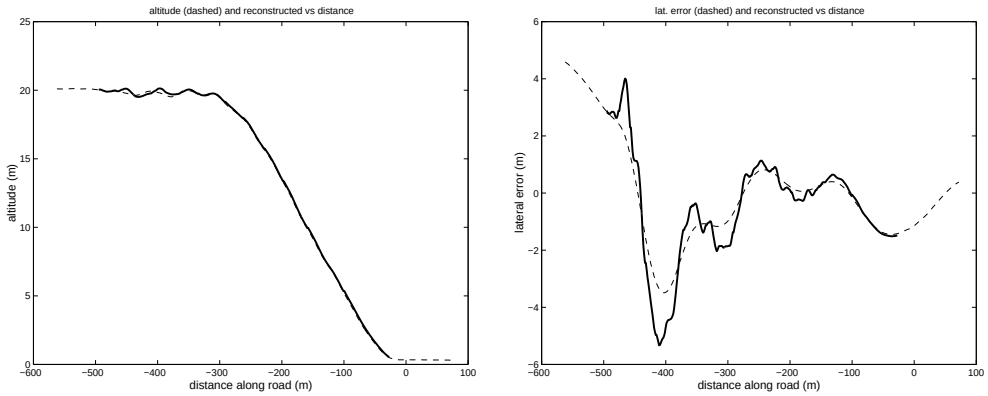


Figure 21: Windy landing image estimation, with altitude (left) and lateral error (right) compared with real values in dashed.

Unité de recherche INRIA Sophia Antipolis
2004, route des Lucioles - BP 93 - 06902 Sophia Antipolis Cedex (France)

Unité de recherche INRIA Lorraine : LORIA, Technopôle de Nancy-Brabois - Campus scientifique
615, rue du Jardin Botanique - BP 101 - 54602 Villers-lès-Nancy Cedex (France)
Unité de recherche INRIA Rennes : IRISA, Campus universitaire de Beaulieu - 35042 Rennes Cedex (France)
Unité de recherche INRIA Rhône-Alpes : 655, avenue de l'Europe - 38330 Montbonnot-St-Martin (France)
Unité de recherche INRIA Rocquencourt : Domaine de Voluceau - Rocquencourt - BP 105 - 78153 Le Chesnay Cedex (France)

Éditeur
INRIA - Domaine de Voluceau - Rocquencourt, BP 105 - 78153 Le Chesnay Cedex (France)
http://www.inria.fr
ISSN 0249-6399